東北大学機関リポジトリ
TOUR
Tohoku University Repository

Hot fusion reactions with deformed nuclei for synthesis of superheavy nuclei: An extension of the fusion-by-diffusion model

Hot fusion reactions with deformed nuclei for synthesis of superheavy nuclei: An extension of the fusion-by-diffusion model

K. Hagino

Department of Physics, Tohoku University, Sendai 980-8578, Japan
and Research Center for Electron Photon Science, Tohoku University, 1-2-1 Mikamine, Sendai 982-0826, Japan

The fusion-by-diffusion model proposed by Swiatecki *et al.* [Phys. Rev. C **71**, 014602 (2005)] has provided a simple and convenient tool to estimate evaporation residue cross sections for superheavy nuclei. I extend this model by taking into account deformation of the target nucleus, and discuss the role of orientation of a deformed target in hot fusion reactions at energies around the Coulomb barrier. To this end, I introduce an injection point for the diffusion process over an inner barrier which depends on the orientation angle. I apply this model to the ^{48}Ca + ^{248}Cm reaction and show that the maximum of evaporation residue cross section appears at an energy slightly above the height of the capture barrier for the side collision, for which the effective inner barrier is considerably lower than that for the tip collision, thus enhancing the diffusion probability. I also discuss the energy dependence of the injection point, and show that a large part of the energy dependence found in the previous analyses can be attributed to the deformation effect of a target nucleus.

I. INTRODUCTION

An investigation of superheavy elements has been one of the most important topics in nuclear physics [1–3]. It is not only related to a fundamental question, "How heavy an element can one define as a nucleus?", but also relevant to many areas of science, including nuclear structure, nuclear reaction, chemistry, and nuclear astrophysics [3]. That is, the stability of superheavy elements is intimately related to the shell structure of superheavy nuclei, and an understanding the reaction dynamics is extremely important for a formation of superheavy nuclei. Furthermore, a good understanding of electronic structure as well as chemical properties is necessary to locate superheavy elements at appropriate positions in a periodic table. Fission of heavy and superheavy elements in r-process nucleosynthesis is also an important topic in nuclear astrophysics in order to investigate the origin of elements found in nature [4].

The heaviest element synthesized so far is the element 118 [5], which was recently named oganesson (Og), together with three other superheavy elements, that is, nihonium (Nh, $Z = 113$) [6,7], moscovium (Mc, $Z = 115$) [7], and tennessine (Ts, $Z = 117$) [8]. These superheavy elements, as well as elements heavier than mendelevium ($Z = 101$), have been synthesized using heavy-ion fusion reactions at energies around the Coulomb barrier [1–3].

It is important to notice here that fusion reactions for superheavy elements are considerably different from fusion in medium-heavy systems [9–14]. Whereas a compound nucleus is formed almost automatically in medium-heavy systems once projectile and target nuclei touch each other [15–19], the strong Coulomb repulsion in the superheavy region makes a touching configuration undergo a reseparation process with a huge probability. This process is referred to as quasifission [20–30],

and has been recognized as a primary cause of fusion inhibition in heavy systems [22,26,31–34]. Since quasifission characteristics often overlap with fission of the compound nucleus (that is, fusion-fission), formation of superheavy elements is usually identified by measuring evaporation residues of the compound nucleus, formation of which is extremely rare in the superheavy region. This makes it extremely challenging to model the formation process of superheavy nuclei and make reliable theoretical predictions for evaporation residue cross sections.

Qualitatively, the significance of quasifission in the different mass regions can be understood in terms of the relative position between the touching configuration and the saddle of the fission barrier. In medium-heavy systems, the saddle appears well outside the touching configuration in deformation space, and thus the compound nucleus is formed with a negligibly small probability of quasifission. On the other hand, in the superheavy region, the strong Coulomb repulsion leads to a lower fission barrier at a smaller deformation as compared to a fission potential in the medium-heavy region (see, e.g., Fig. 7 in Ref. [35]). The touching configuration appears outside the saddle configuration, and thus a compound nucleus is formed only after the fission barrier is overcome, whereas most events lead to quasifission.

Based on this idea, as well as on the timescale of each process, the formation process of evaporation residues can be conceptually divided into a sequence of the following three processes. The first is a process in which two separate nuclei form a touching configuration after overcoming the Coulomb barrier. Here, the channel coupling effects, that is, couplings of the relative motion to several nuclear collective excitations in colliding nuclei as well as several transfer processes, play an important role [15–19]. After two nuclei touch each other, a huge number of nuclear intrinsic motions are activated and the

relative energy is quickly dissipated to internal energies, landing on the right-hand side of the fission barrier for a mononuclear system. The second stage for the formation of evaporation residues is then a diffusion over this inner barrier to form a compound nucleus, with a severe competition with the quasifission process. The third process is a statistical decay of the compound nucleus, with strong competitions between evaporation and fission.

In order to describe such a complicated process, Swiatecki *et al.* have proposed a simple one-dimensional model, that is, the fusion-by-diffusion model [35–37]. In this model, classical fusion cross sections with a Gaussian barrier distribution are employed for the first stage, while the second stage is modeled as a diffusion of a one-dimensional parabolic barrier. Despite model's simplicity, it accounts for experimental cross sections reasonably well for Pb- and Bi-based cold fusion reactions by introducing one adjustable parameter, that is, the injection point for the second stage, or equivalently the height of the fission barrier relative to the touching configuration [35–38].

Subsequently, the fusion-by-diffusion model has been applied also to ^{48}Ca-based hot fusion reactions [39,40]. One of the characteristic features of the ^{48}Ca-based hot fusion reactions [41] is that the corresponding target nuclei are in the actinide region, in which nuclei have a large deformation in the ground state. In the fusion-by-diffusion model, the effect of target deformation has been taken into account only through the Gaussian width for the barrier distribution for the first stage, even though the deformation effect may have been implicitly taken into account by a phenomenological adjustment of the injection point.

In this paper, I extend the fusion-by-diffusion model by taking into account the deformation effect both in the first and the second stages of the evaporation residue formation process. To this end, I introduce the orientation dependence to the injection point. Notice that hot fusion reactions have been, or will be, employed in order to synthesize elements beyond Og, that is, the elements 119 and 120 [42]. The extension discussed in this paper will increase the reliability of the fusion-by-diffusion model and will provide good guidance for future experiments. It will also help in understanding the reaction dynamics of fusion reactions of a deformed nucleus to synthesize superheavy elements. See also Refs. [43–45] for earlier publications which discussed the role of orientation of a deformed target in synthesis of superheavy elements based on a different theoretical model, that is, the dinuclear system model.

The paper is organized as follows. In Sec. II, I summarize the conventional fusion-by-diffusion model of Swiatecki *et al.* in order to clarify the modifications introduced in this paper. In Sec. III, I introduce the extended version of the fusion-by-diffusion model, which takes into account the deformation of a target nucleus. In Sec. IV, I apply the extended version of the model to the ^{48}Ca + ^{248}Cm system and discuss the role of orientation of the deformed ^{248}Cm nucleus. In Sec. V, I discuss the energy dependence of the injection point, and show that the deformation effect leads to a relatively strong energy dependence. I then summarize the paper in Sec. VI.

II. FUSION-BY-DIFFUSION MODEL

Before I discuss the extensions of the fusion-by-diffusion model, I here summarize the current version of the model. To this end, I closely follow Ref. [37], in which the angular momentum dependence of the diffusion and the survival probabilities has been introduced to the original version of the model [35,36]. In this l-dependent version of the fusion-by-diffusion model, evaporation residue cross sections $\sigma_{\rm ER}$ are evaluated as

$$\sigma_{\rm ER}(E) = \frac{\pi}{k^2} \sum_l (2l + 1) T_l(E) P_{\rm fus}(E,l) P_{\rm sur}(E^*,l), \quad (1)$$

where E is the incident energy in the center-of-mass frame and $k = \sqrt{2\mu E/\hbar^2}$ is the corresponding wave number, with μ being the reduced mass in the entrance channel. $T_l(E)$, $P_{\rm fus}(E,l)$, and $P_{\rm sur}(E^*,l)$ are the probabilities for the first, the second, and the third stages, respectively, where E^* is the excitation energy of the compound nucleus. These are the capture probability, that is, the penetrability of the Coulomb barrier, the diffusion probability of the inner fission barrier, and the survival probability of the compound nucleus against fission, respectively. I summarize each probability in the following subsections.

A. Capture probability

In the original version of the fusion-by-diffusion model, capture cross sections,

$$\sigma_{\rm cap}(E) = \frac{\pi}{k^2} \sum_l (2l + 1) T_l(E), \quad (2)$$

are computed as [35,36,46]

$$\sigma_{\rm cap}(E) = \int_{-\infty}^{\infty} dB \, f(B; B_0) \, \sigma_{\rm cl}(E; B), \quad (3)$$

where

$$f(B; B_0) = \frac{1}{\sqrt{2\pi} w} \exp \left[-\frac{(B - B_0)^2}{2w^2} \right] \quad (4)$$

represents the weight factor for a barrier distribution [47] around a mean barrier height B_0, while

$$\sigma_{\rm cl}(E; B) = \pi R_b^2 \left(1 - \frac{B}{E} \right) \theta(E - B) \quad (5)$$

is the classical fusion cross section for the barrier height B and the barrier position R_b. Here, $\theta(E - B)$ is the step function. With the Gaussian function for $f(B; B_0)$, the integral in Eq. (3) can be evaluated analytically as [35,36,46]

$$\sigma_{\rm cap}(E) = \pi R_b^2 \frac{w}{\sqrt{2\pi E}} [\sqrt{\pi} x[1 + {\rm erf}(x)] + e^{-x^2}], \quad (6)$$

with $x \equiv (E - B_0)/(\sqrt{2}w)$, where

$${\rm erf}(x) = \frac{2}{\sqrt{\pi}} \int_0^x e^{-t^2} dt \quad (7)$$

is the error function.

In the l-dependent version of the fusion-by-diffusion model, the capture probability $T_l(E)$ is taken to be the classical one, that is, $T_l(E) = 1$ for $l \leqslant l_{\rm max}$ and 0 for $l > l_{\rm max}$. The maximum

angular momentum, $l_{\max}$, is determined so that the capture cross section so obtained,

$$\sigma_{\mathrm{cap}}(E) = \frac{\pi}{k^2} \sum_{l=0}^{l_{\max}} (2l+1) = \frac{\pi}{k^2} (l_{\max}+1)^2, \qquad (8)$$

coincides approximately with Eq. (6) for given R_b and B_0 [37].

B. Diffusion probability

After two nuclei touch with each other by overcoming the Coulomb barrier, there is an additional inner barrier, which has to be overcome in order to form a superheavy element. In the fusion-by-diffusion model, this process is described as a diffusion of an inverted parabolic potential barrier,

$$V_l(s) = V_{\mathrm{fiss}}(s) + \frac{l(l+1)\hbar^2}{2\mathcal{J}(s)} \sim V_{0l} - C_l(s-s_{\mathrm{sd}})^2, \qquad (9)$$

where s is the coordinate for diffusion, that is, the surface separation between the two spheres [37], $V_{\mathrm{fiss}}(s)$ is the inner (fission) barrier, and $\mathcal{J}(s)$ is the moment of inertia for the mono-nuclear system. The last term in Eq. (9) is due to the parabolic approximation to the potential barrier around the saddle point configuration, s_{sd}.

For a diffusion from an initial configuration s_{inj} at rest, the barrier passing probability at temperature T is given by [48]

$$P_{\mathrm{fus}}(E,l) = \frac{1}{2}\left[1 - \mathrm{erf}\left(\frac{\Delta V_l}{T}\right)\right], \qquad (10)$$

in the overdamped limit, where ΔV_l is the effective barrier height for the second process given by $\Delta V_l = V_l(s_{\mathrm{sd}}) - V_l(s_{\mathrm{inj}})$ (in the fusion-by-diffusion model, the l dependence in each of s_{sd} and s_{inj} is neglected). Notice that the probability is independent of the friction coefficient and the mass parameter in the overdamped limit [48].

For given s and angular momentum l, the temperature T is estimated as

$$T(l,s) = \sqrt{\frac{E^* - V_l(s) - E_{\mathrm{pair}}}{a(s)}}, \qquad (11)$$

where E_{pair} is the pairing energy and $a(s)$ is the level density parameter. The excitation energy E^* is given by $E^* = E - M_{\mathrm{CN}}c^2 + M_P c^2 + M_T c^2$, where M_{CN}, M_P, and M_T are the masses of the compound nucleus, the projectile nucleus, and the target nucleus, respectively. Following Ref. [37], the pairing energy, E_{pair}, is taken to be $21/\sqrt{A}$ MeV for even-even nuclei, where A is the mass number, $10.5/\sqrt{A}$ MeV for odd-mass nuclei, and 0 for odd-odd nuclei. Following again Ref. [37], I take the geometrical mean between the temperature at the saddle configuration and that at the injection point, that is, $T = \sqrt{T(l,s_{\mathrm{sd}})T(l,s_{\mathrm{inj}})}$, for the temperature used in Eq. (10).

See Refs. [35–37] for the parametrization of the inner barrier, $V_{\mathrm{fiss}}(s)$, the moment of inertia, $\mathcal{J}(s)$, and the level density parameter, $a(s)$, used in the fusion-by-diffusion model.

C. Survival probability

In the superheavy region, a compound nucleus formed in a heavy-ion fusion reaction decays primarily by fission.

In the fusion-by-diffusion model, the survival probability against fission is calculated using a simplified statistical model. Assuming that fission competes only with neutron emissions, the survival probability for the N-neutron emission channel is estimated as [37,38,49]

$$P_{\mathrm{sur}}(E^*,l) = \prod_{k=1}^{N-1}\left(\frac{\Gamma_n^{(k)}(E_k^*)}{\Gamma_n^{(k)}(E_k^*) + \Gamma_f^{(k)}(E_k^*)}\left(1 - P_<^{(k)}(E_k^*)\right)\right)$$

$$\times \frac{\Gamma_n^{(N)}(E_N^*)}{\Gamma_n^{(N)}(E_N^*) + \Gamma_f^{(N)}(E_N^*)} P_<^{(N)}(E_N^*), \qquad (12)$$

where $\Gamma_n^{(k)}$ and $\Gamma_f^{(k)}$ are the neutron and the fission widths at an excitation energy E_k^* after emission of $(k-1)$ neutrons, and $1 - P_<^{(k)}$ is the probability of finding the residual nucleus at excitation energies above the threshold of the next chance fission or neutron evaporation. Notice that $\Gamma_n^{(k)}$, $\Gamma_f^{(k)}$, and $P_<^{(k)}$ depend on the angular momentum l, but this is not expressed explicitly in Eq. (12) for simplicity of the notation.

The decay widths, $\Gamma_n^{(k)}$ and $\Gamma_f^{(k)}$, as well as the probability $P_<^{(k)}$ are expressed in terms of the level density, the fission barrier, and the one-neutron separation energy. See Refs. [37,38,49] for their explicit forms.

III. EXTENSION TO DEFORMED SYSTEMS

I now discuss the extension of the fusion-by-diffusion model to deformed systems. In the original version of the model discussed in the previous section, the effect of deformation is taken into account only through the Gaussian width, w, in Eq. (4) as [35,37]

$$w \propto \sqrt{\frac{R_P^2 \beta_{2P}^2}{4\pi} + \frac{R_T^2 \beta_{2T}^2}{4\pi} + w_0^2}, \qquad (13)$$

where w_0 is a constant and β_{2P} and β_{2T} are the quadrupole deformation parameters of the projectile and the target, respectively. The deformation effect may also be included implicitly when the injection point, s_{inj}, is adjusted phenomenologically.

In this paper, I introduce the deformation effect more explicitly to the model. To this end, I write the evaporation residue cross sections as [17]

$$\sigma_{\mathrm{ER}}(E) = \int_0^1 d(\cos\theta)\, \sigma_{\mathrm{ER}}(E;\theta), \qquad (14)$$

where θ is the orientation angle of a deformed target with respect to the beam direction, and $\sigma_{\mathrm{ER}}(E;\theta)$ is the evaporation residue cross section for a fixed value of θ given by

$$\sigma_{\mathrm{ER}}(E;\theta) = \frac{\pi}{k^2}\sum_l (2l+1)T_l(E,\theta)P_{\mathrm{fus}}(E,l,\theta)P_{\mathrm{sur}}(E^*,l). \qquad (15)$$

This formula is based on the isocentrifugal approximation to the angular momentum coupling [17] and on an assumption that the moment of inertia for the rotational motion is so large (therefore the energy of the first 2^+ state is so small) that the orientation angle of the deformed target nucleus is fixed during fusion [17], which is well fulfilled in the actinide region.

Notice that the survival probability, P_{sur}, remains the same as in the original version of the model, since it is related to properties of the compound nucleus, for which the memory of the entrance channel is assumed to be lost. On the other hand, the deformation effect modifies the capture probability, T_l, as well as the diffusion probably, P_{fus}. I will discuss below how the orientation effect can be taken into account in these probabilities.

A. Capture probability

In order to take into account the deformation effect on the capture probability, T_l, I introduce a deformed nuclear potential of the Woods-Saxon type for the relative motion between the target and the projectile nuclei,

$$V_N(r,\theta) = -\frac{V_0}{1 + \exp[\{r - R_0 - R_T \sum_\lambda \beta_{\lambda T} Y_{\lambda 0}(\theta)\}/a]},$$
(16)

where V_0, R_0, and a are the depth, the radius, and the diffuseness parameters, respectively, and $\beta_{\lambda T}$ are the deformation parameters of the target nucleus. The Coulomb part of the potential is also deformed as [17,50]

$$
V_C(r,\theta) = \frac{Z_P Z_T e^2}{r}
$$
$$
+ \frac{3 Z_P Z_T e^2}{5} \frac{R_T^2}{r^3}\left(\beta_{2T} + \frac{2}{7}\sqrt{\frac{5}{\pi}}\beta_{2T}^2\right)Y_{20}(\theta)
$$
$$
+ \frac{3 Z_P Z_T e^2}{9} \frac{R_T^4}{r^5}\left(\beta_{4T} + \frac{9}{7\sqrt{\pi}}\beta_{2T}^2\right)Y_{40}(\theta)
$$
$$
+ \frac{3 Z_P Z_T e^2}{13} \frac{R_T^6}{r^7}\beta_{6T} Y_{60}(\theta),
$$
(17)

to the second order in the quadrupole deformation parameter, β_{2T}, and the first order in the hexadecapole and the hexacontatetrapole deformation parameters, β_{4T} and β_{6T}, respectively. The total potential for angular momentum l reads

$$V(r,\theta) = V_N(r,\theta) + V_C(r,\theta) + \frac{l(l+1)\hbar^2}{2\mu r^2},$$
(18)

where the last term is the centrifugal potential.

I use the parabolic approximation to the potential, $V(r,\theta)$, that is, I expand the potential as

$$V(r,\theta) \sim V_b(l,\theta) - \frac{1}{2}\mu\Omega(l,\theta)^2[r - R_b(l,\theta)]^2$$
(19)

around the position of the Coulomb barrier, $R_b(l,\theta)$, for a fixed value of θ. The penetrability of this potential is then computed as [17]

$$T_l(E,\theta) = \frac{1}{1 + \exp\left[\frac{2\pi}{\hbar\Omega(l,\theta)}[V_b(l,\theta) - E]\right]}.$$
(20)

B. Diffusion probability

The deformation effect implies that one would have to consider a diffusion in a multidimensional inner barrier, V_{fiss}, with deformation and orientation degrees of freedom, for the second stage of the evaporation residue formation process.
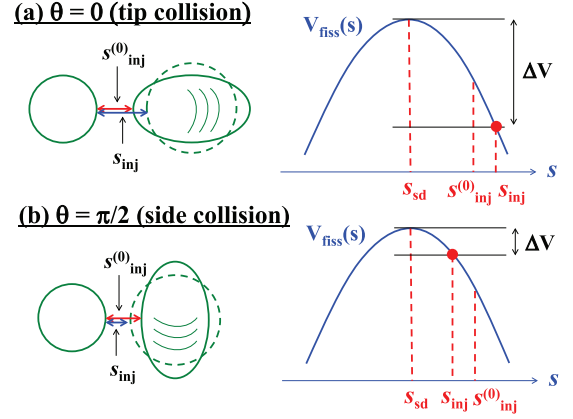

FIG. 1. A schematic illustration of the angular dependence of the injection distance, $s_{inj}(\theta)$. The upper and the lower figures show the configuration with $\theta = 0$ and $\theta = \pi/2$, respectively, where θ is the orientation angle for a prolately deformed nucleus.

Even though this is certainly an interesting future work, I prefer to retain here the simplicity of the fusion-by-diffusion model and thus use a one-dimensional potential. Instead, I introduce the orientation dependence to the injection point based on the notion of compactness for quasifission [26,51–55].

Suppose that the target and the projectile nuclei are separated with the distance L at the injection point. For a spherical target, the separation distance is then given by

$$L = R_P + R_T + s_{inj}^{(0)}.$$
(21)

When the target nucleus is deformed, the radius R_T is replaced by $R_T(\theta) = R_T[1 + \sum_\lambda \beta_{\lambda T} Y_{\lambda 0}(\theta)]$. Substituting this expression in Eq. (21), one obtains

$$L(\theta) = R_P + R_T(\theta) + s_{inj}^{(0)},$$
(22)

$$= R_P + R_T + s_{inj}^{(0)} + R_T \sum_\lambda \beta_{\lambda T} Y_{\lambda 0}(\theta).$$
(23)

This implies that the orientation dependent injection parameter is given by

$$s_{inj}(\theta) = L(\theta) - R_P - R_T = s_{inj}^{(0)} + R_T \sum_\lambda \beta_{\lambda T} Y_{\lambda 0}(\theta).$$
(24)

This is schematically illustrated in Fig. 1. The diffusion probability is then given by

$$P_{fus}(E,l,\theta) = \frac{1}{2}\left[1 - \mathrm{erf}\left(\frac{\Delta V_l(\theta)}{T(\theta)}\right)\right],$$
(25)

where both the effective barrier height, ΔV_l, and the temperature, T, depend on the angle θ through the angle dependent injection point, $s_{inj}(\theta)$. A similar idea was employed also in Ref. [56] in more realistic Langevin calculations.

IV. APPLICATION TO THE ^{48}Ca + ^{248}Cm REACTION

Let us now apply the extended fusion-by-diffusion model discussed in the previous section to the ^{48}Ca + ^{248}Cm reaction. I choose this system as a representative example for hot fusion reactions, and also because the barrier distribution for the
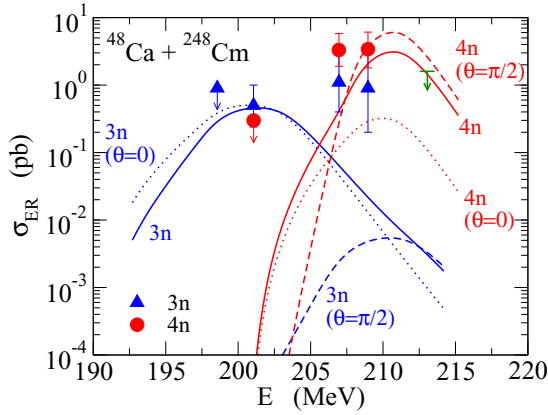
FIG. 2. The evaporation residue cross sections for the ^{48}Ca + ^{248}Cm system as a function of the incident energy in the center-of-mass frame obtained with the extended fusion-by-diffusion model with deformations of the target nucleus. Eq. (26) is used for the energy dependence of the injection point. The dotted and the dashed lines show the cross sections for the orientation angles of $\theta = 0$ and $\theta = \pi/2$, respectively, while the solid lines are obtained by taking an average over all the angles θ. The experimental data are taken from Refs. [64,65].

capture process has recently been measured for this system [57] using quasielastic scattering [58,59]. The theoretical analysis for the measured barrier distribution has clearly shown that the maximum of the evaporation residue cross sections for this system appears at an energy slightly above the barrier height for the *side* collision, in good agreement with the notion of compactness [26,51–55]. The aim of this section is to gain a deeper insight into the effect of orientation of the deformed ^{248}Cm nucleus by reanalyzing the evaporation residue cross sections using the extended fusion-by-diffusion model.

In the calculation presented below, I use the deformation parameters of $\beta_{2T} = 0.297$, $\beta_{4T} = 0.039$, and $\beta_{6T} = -0.035$ together with the radius of $R_T = 1.2A_T^{1/3}$ fm for the entrance channel. The value of β_{2T} is estimated from the measured electric transition probability [60], while the values of β_{4T} and β_{6T} are taken from Ref. [61]. For the Woods-Saxon potential, I use the parameters $V_0 = 70$ MeV, $R_0 = 1.18 \times (48^{1/3} + 248^{1/3})$ fm, and $a = 0.69$ fm, which are similar to the ones used in Ref. [57] for the coupled-channels analysis for the quasielastic barrier distribution for this system, with a slight readjustment in order to reproduce the measured capture cross sections [62]. The deformation parameters and the shell correction energies, both at the ground state and at the saddle point, as well as the ground state masses and the fission barrier heights, are all taken from Ref. [63]. This mass table lists the values only for even-even nuclei, and thus for odd-mass nuclei I take an average of the values for the neighboring nuclei. I assume that the shell correction energy is negligible at the injection point. Following Refs. [37,39], I introduce a liner energy dependence to the injection point, $s_{\mathrm{inj}}^{(0)}$, in Eq. (24), which is specified below.

The solid lines in Fig. 2 show the evaporation residue cross sections obtained with

$$s_{\mathrm{inj}}^{(0)} = 4.698\mathrm{fm} - 0.16(E - B_0)\ \mathrm{fm/MeV}, \qquad (26)$$

where the reference barrier height, B_0, is given by [37]

$$B_0 = 0.853315z + 0.0011695z^2 - 0.000001544z^3\ \mathrm{MeV}, \qquad (27)$$

with $z = Z_P Z_T /(A_P^{1/3} + A_T^{1/3})$. In order to compare with the experimental data [64,65], I smear the calculated cross sections as

$$\bar{\sigma}_{\mathrm{ER}}(E) = \frac{1}{\Delta E} \int_{E-\Delta E/2}^{E+\Delta E/2} \sigma_{\mathrm{ER}}(E')dE', \qquad (28)$$

in order to take into account a loss of the beam energy in the target material with a finite thickness [37]. According to Refs. [64,65], I take $\Delta E = 5.4$ and 3.4 MeV for the 3n and 4n evaporation channels, respectively, even though different values for ΔE should be used for different experimental runs. The figure also shows the cross section for $\theta = 0$ and $\theta = \pi/2$ by the dotted and the dashed lines, respectively [see Eq. (15)]. One can see that the 4n channel is mainly due to the side collision with $\theta = \pi/2$, while the 3n channel is mainly due to the tip collision with $\theta = 0$. The former result is consistent with the earlier experimental conclusions in
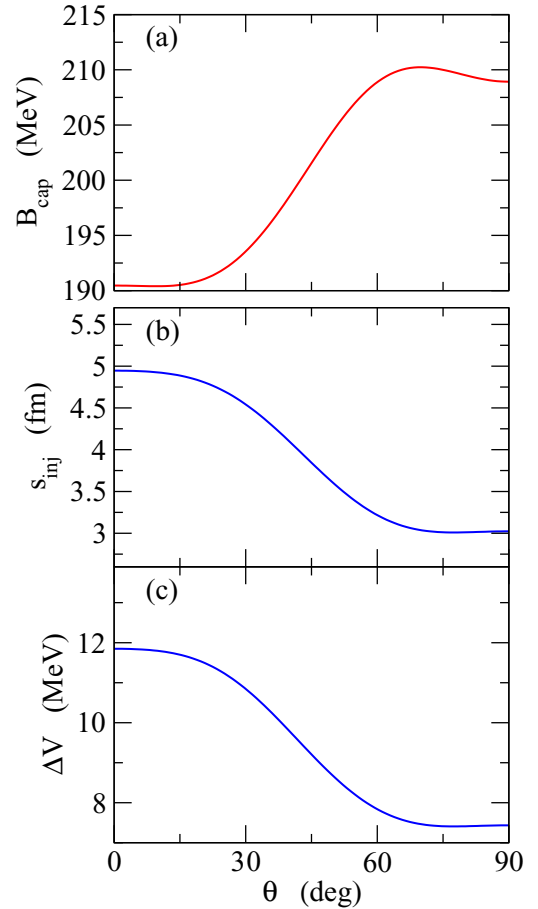

FIG. 3. The dependence of (a) the capture barrier height, (b) the injection distance, and (c) the height of the diffusion barrier on the orientation angle of the deformed target nucleus for the ^{48}Ca + ^{248}Cm reaction. The injection distance and the height of the diffusion barrier are evaluated at energy $E = 215$ MeV in Eq. (26).

Refs. [26,51–54,57]. In order to demonstrate the validity of the present model, I also show the result for the ^{48}Ca $+$ ^{238}U system in the Appendix.

The energy dependence of the relative contribution for the side and the tip collisions can be understood in terms of the angle dependence of the capture and the diffusion barriers. The top panel of Fig. 3 shows the height of the capture barrier as a function of the orientation angle. For nuclei with prolate deformation, the barrier is lower for the tip collision ($\theta = 0$) and increases with θ (the figure shows a nonmonotonic behavior due to the finite value of β_6 deformation). Therefore, the side collision is suppressed at low energies. The middle and the bottom panels show the injection distance and the barrier height for the diffusion process, respectively, at $E = 215$ MeV. The injection distance is small for the side collision, and thus the diffusion barrier is low. This leads to an enhancement of the diffusion probability for the side collision as compared to that for the tip collision. The side collision then becomes dominant at high energies, where the suppression due to the capture process is small.

In order to demonstrate this more explicitly, Figs. 4 and 5 show the capture, the diffusion, and the compound nucleus formation probabilities for $l = 0$ as a function of the orientation angle, θ, at $E = 200$ and 211 MeV, respectively. Here, the compound nucleus formation probability is defined as a product of the capture and the diffusion probabilities. For $E = 200$ MeV shown in Fig. 4, the capture barrier is higher than the incident energy for $\theta > 43$ deg [see Fig. 3(a)], and the capture probability drops off abruptly in this range of orientation angle. The contribution of the side collision is
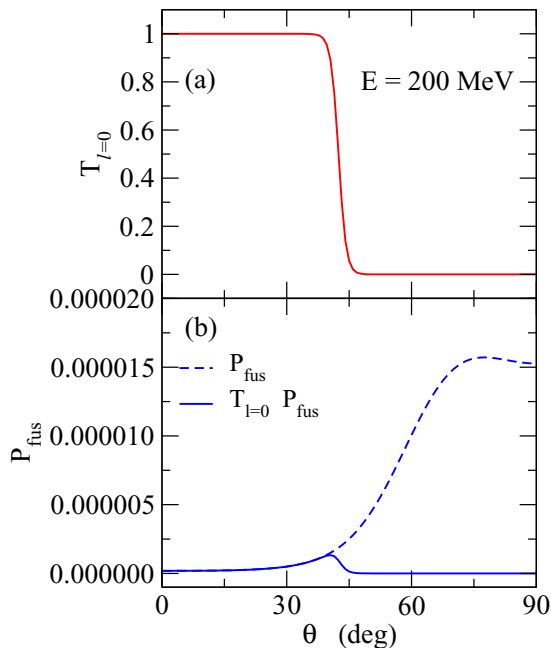

FIG. 4. The dependence of (a) the capture probability, $T_{l=0}$, and (b) the diffusion probability, P_{fus}, on the orientation angle of the deformed target nucleus for the s-wave ^{48}Ca $+$ ^{248}Cm reaction at $E = 200$ MeV. In panel (b), the compound nucleus formation probability, defined as a product of $T_{l=0}$ and P_{fus}, is also shown by the solid line.
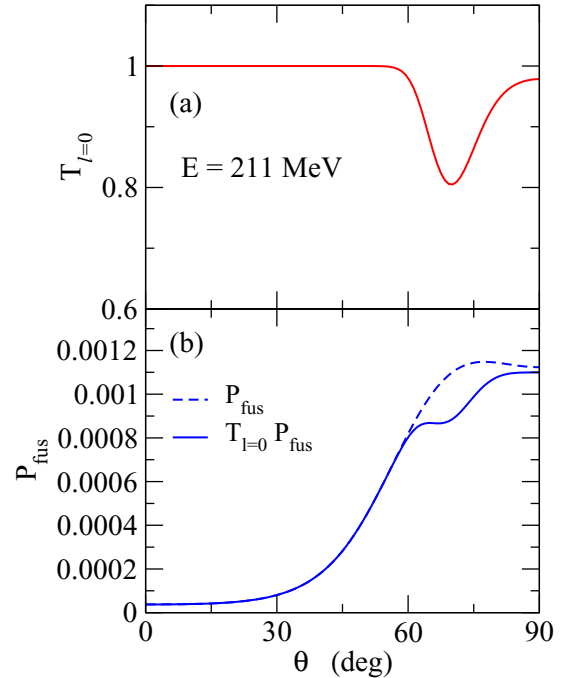

FIG. 5. Same as Fig. 4, but at $E = 211$ MeV.

then negligible even though the diffusion probability itself is relatively large, as shown in the lower panel of Fig. 4. On the other hand, for $E = 211$ MeV shown in Fig. 5, the capture probability is close to unity except for the angles around $\theta \sim 70$ deg (again, the nonmonotonic behavior is due to the finite value of β_6), and the side collision competes well with the tip collision in the capture stage of the reaction. The side collision then gives the largest contribution to the compound nucleus formation, since the diffusion probability is large due to a small injection distance. A qualitatively similar conclusion has been obtained also with the dinuclear system model [45].

V. ENERGY DEPENDENCE OF THE INJECTION DISTANCE

The evaporation residue cross sections for the ^{48}Ca $+$ ^{248}Cm system obtained with the original version of the fusion-by-diffusion model are shown in Fig. 2(d) in Ref. [39]. In order to draw this figure, the authors of Ref. [39] used the parametrization of the injection distance given by

$$s_{\mathrm{inj}} = 4.09\mathrm{fm} - 0.192(E - B_0) \text{ fm/MeV}. \qquad (29)$$

Notice that this energy dependence of the injection distance is much stronger than the one used for cold fusion reactions, that is, $s_{\mathrm{inj}} = 2.30\mathrm{fm} - 0.062(E - B_0)$ fm/MeV [37].

A similar quality of the result to the one obtained with the original version of the model can be obtained with the extended version of the model discussed in this paper using

$$s_{\mathrm{inj}}^{(0)} = 3.457\mathrm{fm} - 0.062(E - B_0) \text{ fm/MeV}, \qquad (30)$$

as shown by the solid lines in the upper panel of Fig. 6. Notice that this has the same energy dependence of s_{inj} as the one for cold fusion reactions discussed in Ref. [37]. If the angle
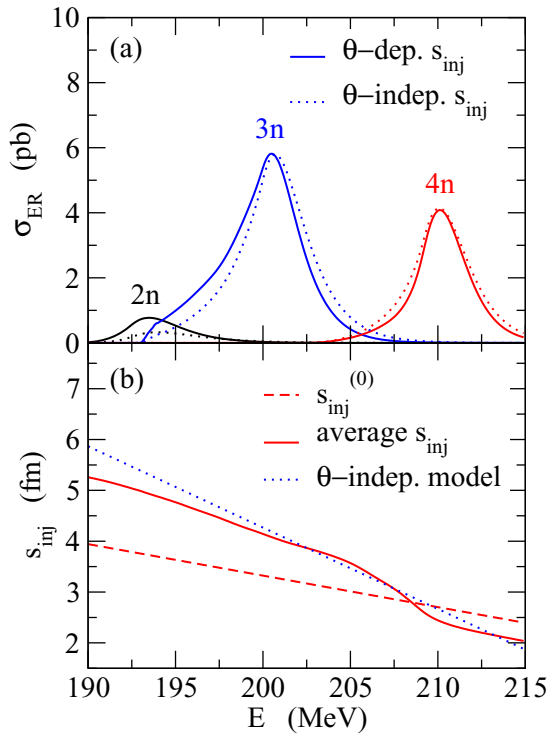
FIG. 6. Upper panel: The evaporation residue cross sections for the ^{48}Ca + ^{248}Cm system obtained with the extended version of the fusion-by-diffusion model with Eq. (30) (the solid lines), in comparison with the results obtained by neglecting the angle dependence of the injection distance (the dotted lines). Lower panel: The energy dependence of the injection distance. The dashed line shows the energy dependence given by Eq. (30), while the solid line takes into account the deformation effect with Eq. (32). The dotted line shows the energy dependence for the angle independent model, which corresponds to the dotted lines in the upper panel.

dependence of $s_{\mathrm{inj}}(\theta)$ is disregarded in the present model, similar results are obtained with a stronger dependence, that is,

$$s_{\mathrm{inj}}(\theta) = 4.613\,\mathrm{fm} - 0.16(E - B_0)\,\mathrm{fm/MeV}, \tag{31}$$

as shown by the dotted lines in the figure. Therefore, the energy dependence of the injection distance is indeed weakened if the deformation effect is explicitly taken into account.

In order to discuss this point more clearly, I take an average of $s_{\mathrm{inj}}(\theta)$ with the total evaporation residue cross sections for each angle θ, $\sigma_{\mathrm{ER}}(\theta)$, as a weight factor. That is, I define the average injection distance as

$$\bar{s}_{\mathrm{inj}}(E) \equiv \frac{\int_0^1 d(\cos\theta) s_{\mathrm{inj}}(\theta)\sigma_{\mathrm{ER}}(E;\theta)}{\int_0^1 d(\cos\theta)\sigma_{\mathrm{ER}}(E;\theta)}. \tag{32}$$

This quantity is shown by the solid line in the lower panel of Fig. 6. For a comparison, the figure also shows the energy dependences given by Eqs. (30) and (31) with the dashed and the dotted lines, respectively. One can clearly see from the figure that the angle dependence of the injection distance provides a strong energy dependence of an effective injection distance, which is compatible with the energy dependence obtained with the angle-independent model shown by the dotted line.

Evidently, the strong energy dependence found in Ref. [39] for hot fusion reactions mocks up the deformation effect of the target nuclei to a large extent, which is not included explicitly in the original version of the fusion-by-diffusion model.

VI. SUMMARY

By taking into account the effects of deformation of the target nucleus, I have extended the fusion-by-diffusion model of Swiatecki *et al.* for heavy-ion fusion reactions to synthesize superheavy elements. To this end, I have introduced the angle dependence to the injection distance, based on the notion of compactness for quasifission. I have also used a barrier distribution for the capture process that is consistent with the rotational coupling of a deformed nucleus. I have applied the extended version of the fusion-by-diffusion model to the hot fusion reaction ^{48}Ca + ^{248}Cm as a representative example and found that the maximum of evaporation residue cross sections appears at an energy slightly above the Coulomb barrier for the side collision. At this energy, the capture probability is close to unity, while the diffusion probability is large for the side collision due to a compactness of the touching configuration. At lower energies, the side collision is largely suppressed because of a high capture barrier, and the tip collision gives an important contribution.

I have also discussed the energy dependence of the injection distance. I have argued that a strong energy dependence shows up when the deformation effect is converted to an effective energy dependence. This observation is consistent with the strong energy dependence found in the previous analyses for hot fusion reactions with the original version of the fusion-by-diffusion model.

In this paper, following the philosophy of the fusion-by-diffusion model, I considered a diffusion of a simple one-dimensional inner barrier, for which the deformation effect is taken into account only through the injection point for diffusion. In reality, however, it is not obvious at all how the diffusion path is evolved in a multidimensional energy surface with deformation and orientation degrees of freedom. In particular, as the nuclear deformation is a quantal effect, it is expected that the deformation will be reduced or even disappears during the heat-up process after the contact of two colliding nuclei. It would remain a theoretical challenge to model the shape evolution of the dinuclear system towards a compound nucleus by taking into account the gradual change of the deformation in a hot target-like nucleus. To address this question, one would need to develop a quantum theory of friction, such as the ones discussed in Ref. [66]. Obviously, much more work is necessary towards this goal and to gain a deep insight into the reaction dynamics of heavy-ion fusion reactions for the synthesis of superheavy nuclei.

APPENDIX: APPLICATION OF THE EXTENDED FUSION-BY-DIFFUSION MODEL TO THE ^{48}Ca + ^{238}U REACTION

In order to demonstrate the validity of the extended fusion-by-diffusion model proposed in this paper, in this Appendix I apply it to another system besides the ^{48}Ca + ^{248}Cm system discussed in Sec. IV, that is, the ^{48}Ca + ^{238}U reaction. To this end, I use the deformation parameters $\beta_{2T} = 0.289$, $\beta_{4T} = 0.098$, and $\beta_{6T} = -0.021$ [61] together with the radius $R_T = 1.2A_T^{1/3}$ fm. For the Woods-Saxon potential, I use the parameters $V_0 = 400$ MeV, $R_0 = 0.95 \times (48^{1/3} + 238^{1/3})$ fm, and $a = 1.0$ fm in order to reproduce the measured capture cross sections for this system [62].

Figure 7 shows the evaporation residue cross sections thus obtained. To this end, I used Eq. (30) for the injection distance, $s_{\text{inj}}^{(0)}$. As can be seen, the present model yields a fair agreement with the experimental data, indicating the validity of the present approach. Moreover, the 3n and the 4n evaporation channels are dominated by the tip and the side collisions, respectively, which is similar to the conclusion for the ^{48}Ca + ^{248}Cm system shown in Sec. IV.

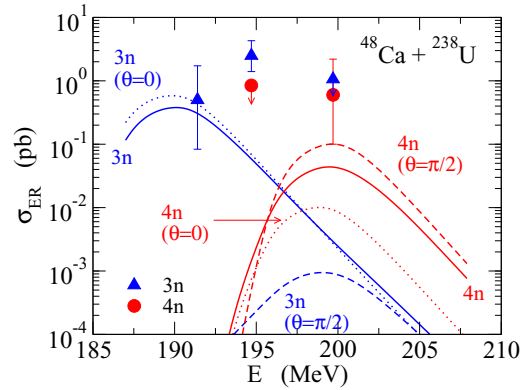One would obtain a better agreement with the experimental data by adjusting the injection distance. Notice that this

FIG. 7. Same as Fig. 2, but for the ^{48}Ca + ^{238}U reaction. The experimental data are taken from Ref. [65].

is related to a question of whether one can find a global parametrization for the injection distance that works for all hot fusion reactions. Apparently, this requires a systematic study, and this is beyond the scope of the present paper. The results of such a systematic study will be reported in a separate publication.

[1] S. Hofmann and G. Münzenberg, Rev. Mod. Phys. **72**, 733 (2000).

[2] J. H. Hamilton, S. Hofmann, and Y. T. Oganessian, Annu. Rev. Nucl. Part. Sci. **63**, 383 (2013).

[3] *Special Issue on Superheavy Elements*, edited by C. E. Düllmann, R.-D. Herzberg, W. Nazarewicz, and Y. Oganessian, Nucl. Phys. A **944**, 1 (2015).

[4] M. R. Mumpower, T. Kawano, T. M. Sprouse, N. Vassh, E. M. Holmbeck, R. Surman, and P. Möller, arXiv:1802.04398.

[5] Yu. Ts. Oganessian *et al.*, Phys. Rev. C **74**, 044602 (2006).

[6] K. Morita *et al.*, J. Phys. Soc. Jpn. **73**, 2593 (2004); **76**, 045001 (2007); **81**, 103201 (2012).

[7] Yu. Ts. Oganessian *et al.*, Phys. Rev. C **69**, 021601(R) (2004); **76**, 011601(R) (2007).

[8] Yu. Ts. Oganessian *et al.*, Phys. Rev. Lett. **104**, 142502 (2010).

[9] V. I. Zagrebaev and W. Greiner, Nucl. Phys. A **944**, 257 (2015).

[10] V. I. Zagrebaev, Y. Aritomo, M. G. Itkis, Y. T. Oganessian, and M. Ohta, Phys. Rev. C **65**, 014607 (2001).

[11] Y. Aritomo, T. Wada, M. Ohta, and Y. Abe, Phys. Rev. C **59**, 796 (1999).

[12] C. W. Shen, G. Kosenko, and Y. Abe, Phys. Rev. C **66**, 061602 (2002).

[13] N. V. Antonenko, E. A. Cherepanov, A. K. Nasirov, V. P. Permajakov, and V. V. Volkov, Phys. Lett. B **319**, 425 (1993).

[14] A. Diaz-Torres, G. G. Adamian, N. V. Antonenko, and W. Scheid, Phys. Rev. C **64**, 024604 (2001).

[15] A. B. Balantekin and N. Takigawa, Rev. Mod. Phys. **70**, 77 (1998).

[16] M. Dasgupta, D. J. Hinde, N. Rowley, and A. M. Stefanini, Annu. Rev. Nucl. Part. Sci. **48**, 401 (1998).

[17] K. Hagino and N. Takigawa, Prog. Theor. Phys. **128**, 1061 (2012).

[18] B. B. Back, H. Esbensen, C. L. Jiang, and K. E. Rehm, Rev. Mod. Phys. **86**, 317 (2014).

[19] G. Montagnoli and A. M. Stefanini, Eur. Phys. J. A **53**, 169 (2017).

[20] J. Tōke, R. Bock, G. X. Dai, A. Gobbi, S. Gralla, K. D. Hildenbrand, J. Kuzminski, W. F. J. Müller, A. Olmi, and H. Stelzer, Nucl. Phys. A **440**, 327 (1985).

[21] B. B. Back, Phys. Rev. C **31**, 2104 (1985).

[22] D. J. Hinde, R. G. Thomas, R. du Rietz, A. Diaz-Torres, M. Dasgupta, M. L. Brown, M. Evers, L. R. Gasques, R. Rafiei, and M. D. Rodriguez, Phys. Rev. Lett. **100**, 202701 (2008).

[23] R. du Rietz, E. Williams, D. J. Hinde, M. Dasgupta, M. Evers, C. J. Lin, D. H. Luong, C. Simenel, and A. Wakhle, Phys. Rev. C **88**, 054618 (2013).

[24] E. Williams, D. J. Hinde, M. Dasgupta, R. du Rietz, I. P. Carter, M. Evers, D. H. Luong, S. D. McNeil, D. C. Rafferty, K. Ramachandran, and A. Wakhle, Phys. Rev. C **88**, 034611 (2013).

[25] J. Khuyagbaatar, D. J. Hinde, I. P. Carter, M. Dasgupta, C. E. Düllmann, M. Evers, D. H. Luong, R. du Rietz, A. Wakhle, E. Williams, and A. Yakushev, Phys. Rev. C **91**, 054608 (2015).

[26] D. J. Hinde, D. Y. Jeung, E. Prasad, A. Wakhle, M. Dasgupta, M. Evers, D. H. Luong, R. du Rietz, C. Simenel, E. C. Simpson, and E. Williams, Phys. Rev. C **97**, 024616 (2018).

[27] E. M. Kozulin, G. N. Knyazheva, K. V. Novikov, I. M. Itkis, M. G. Itkis, S. N. Dmitriev, Yu. Ts. Oganessian, A. A. Bogachev, N. I. Kozulina, I. Harca, W. H. Trzaska, and T. K. Ghosh, Phys. Rev. C **94**, 054613 (2016).

[28] G. N. Knyazheva, E. M. Kozulin, R. N. Sagaidak, A. Yu. Chizhov, M. G. Itkis, N. A. Kondratiev, V. M. Voskressensky, A. M. Stefanini, B. R. Behera, L. Corradi, E. Fioretto, A. Gadea,

A. Latina, S. Szilner, M. Trotta, S. Beghini, G. Montagnoli, F. Scarlassara, F. Haas, N. Rowley, P. R. S. Gomes, and A. Szanto de Toledo, Phys. Rev. C **75**, 064602 (2007).

[29] K. Nishio, S. Mitsuoka, I. Nishinaka, H. Makii, Y. Wakabayashi, H. Ikezoe, K. Hirose, T. Ohtsuki, Y. Aritomo, and S. Hofmann, Phys. Rev. C **86**, 034608 (2012).

[30] A. N. Andreyev, K. Nishio, and K.-H. Schmidt, Rep. Prog. Phys. **81**, 016301 (2018).

[31] C.-C. Sahm, H.-G. Clerc, K.-H. Schmidt, W. Reisdorf, P. Armbruster, F. P. Hessberger, J. G. Keller, G. Münzenberg, and D. Vermeulen, Nucl. Phys. A **441**, 316 (1985).

[32] D. J. Hinde, M. Dasgupta, and A. Mukherjee, Phys. Rev. Lett. **89**, 282701 (2002).

[33] A. C. Berriman, D. J. Hinde, M. Dasgupta, C. R. Morton, R. D. Butt, and J. O. Newton, Nature (London) **413**, 144 (2001).

[34] R. Yanez, W. Loveland, J. S. Barrett, L. Yao, B. B. Back, S. Zhu, and T. L. Khoo, Phys. Rev. C **88**, 014606 (2013).

[35] W. J. Swiatecki, K. Siwek-Wilczynska, and J. Wilczynski, Phys. Rev. C **71**, 014602 (2005).

[36] W. J. Swiatecki, K. Siwek-Wilczynska, and J. Wilczynski, Acta Phys. Pol. B **34**, 2049 (2003).

[37] T. Cap, K. Siwek-Wilczynska, and J. Wilczynski, Phys. Rev. C **83**, 054602 (2011).

[38] T. Ichikawa and A. Iwamoto, J. Phys. Soc. Jpn. **79**, 074201 (2010).

[39] K. Siwek-Wilczynska, T. Cap, M. Kowal, A. Sobiczewski, and J. Wilczynski, Phys. Rev. C **86**, 014611 (2012).

[40] T. Cap, K. Siwek-Wilczynska, M. Kowal, and J. Wilczynski, Phys. Rev. C **88**, 037603 (2013).

[41] Yu. Ts. Oganessian and V. K. Utyonkov, Nucl. Phys. A **944**, 62 (2015).

[42] C. E. Düllmann, EPJ Web Conf. **163**, 00015 (2017).

[43] A. Nasirov, A. Fukushima, Y. Toyoshima, Y. Aritomo, A. Muminov, S. Kaladarov, and R. Utamuratov, Nucl. Phys. A **759**, 342 (2005).

[44] N. Wang, J.-q. Li, and E.-g. Zhao, Phys. Rev. C **78**, 054607 (2008).

[45] L. Zhu, Z.-Q. Feng, C. Li, and F.-S. Zhang, Phys. Rev. C **90**, 014612 (2014).

[46] K. Siwek-Wilczynska and J. Wilczynski, Phys. Rev. C **69**, 024611 (2004).

[47] N. Rowley, G. R. Satchler, and P. H. Stelson, Phys. Lett. B **254**, 25 (1991).

[48] Y. Abe, D. Boilley, B. G. Giraud, and T. Wada, Phys. Rev. E **61**, 1125 (2000).

[49] T. Cap, K. Siwek-Wilczynska, I. Skwira-Chalot, and J. Wilczynski, Acta Phys. Pol. B **43**, 297 (2012).

[50] K. Hagino, N. Rowley, and A. T. Kruppa, Comput. Phys. Commun. **123**, 143 (1999).

[51] D. J. Hinde, M. Dasgupta, J. R. Leigh, J. P. Lestone, J. C. Mein, C. R. Morton, J. O. Newton, and H. Timmers, Phys. Rev. Lett. **74**, 1295 (1995).

[52] D. J. Hinde, M. Dasgupta, J. R. Leigh, J. C. Mein, C. R. Morton, J. O. Newton, and H. Timmers, Phys. Rev. C **53**, 1290 (1996).

[53] K. Nishio, H. Ikezoe, S. Mitsuoka, I. Nishinaka, Y. Nagame, Y. Watanabe, T. Ohtsuki, K. Hirose, and S. Hofmann, Phys. Rev. C **77**, 064607 (2008).

[54] K. Nishio, H. Ikezoe, S. Mitsuoka, and J. Lu, Phys. Rev. C **62**, 014602 (2000).

[55] N. Rowley, N. Grar, and M. Trotta, Phys. Rev. C **76**, 044612 (2007).

[56] Y. Aritomo, K. Hagino, K. Nishio, and S. Chiba, Phys. Rev. C **85**, 044614 (2012).

[57] T. Tanaka, Y. Narikiyo, K. Morita, K. Fujita, D. Kaji, K. Morimoto, S. Yamaki, Y. Wakabayashi, K. Tanaka, M. Takeyama, A. Yoneda, H. Haba, Y. Komori, S. Yanou, B. J.-P. Gall, Z. Asfari, H. Faure, H. Hasebe, M. Huang, J. Kanaya, M. Murakami, A. Yoshida, T. Yamaguchi, F. Tokanai, T. Yoshida, S. Yamamoto, Y. Yamano, K. Watanabe, S. Ishizawa, M. Asai, R. Aono, S. Goto, K. Katori, and K. Hagino, J. Phys. Soc. Jpn. **87**, 014201 (2018).

[58] H. Timmers, J. R. Leigh, M. Dasgupta, D. J. Hinde, R. C. Lemmon, J. C. Mein, C. R. Morton, J. O. Newton, and N. Rowley, Nucl. Phys. A **584**, 190 (1995).

[59] K. Hagino and N. Rowley, Phys. Rev. C **69**, 054610 (2004).

[60] S. Raman, C. W. Nestor, Jr., and P. Tikkanen, At. Data Nucl. Data Tables **78**, 1 (2001).

[61] P. Möller, A. J. Sierk, T. Ichikawa, and H. Sagawa, At. Data Nucl. Data Tables **109–110**, 1 (2016).

[62] E. M. Kozulin, G. N. Knyazheva, I. M. Itkis, M. G. Itkis, A. A. Bogachev, E. V. Chernysheva, L. Krupa, F. Hanappe, O. Dorvaux, L. Stuttge, W. H. Trzaska, C. Schmitt, and G. Chubarian, Phys. Rev. C **90**, 054608 (2014).

[63] M. Kowal, P. Jachimowicz, and J. Skalski, arXiv:1203.5013.

[64] S. Hofmann *et al.*, Eur. Phys. J. A **48**, 62 (2012).

[65] Yu. Ts. Oganessian *et al.*, Phys. Rev. C **70**, 064609 (2004); **63**, 011301 (2000).

[66] M. Tokieda and K. Hagino, Phys. Rev. C **95**, 054604 (2017).